Journal of Molecular Catalysis A: Chemical 356 (2012) 137–143

Contents lists available at SciVerse ScienceDirect

Journal of Molecular Catalysis A: Chemical

journal homepage: www.elsevier.com/locate/molcata

Microwave-assisted rapid synthesis of anatase TiO_2 nanocrystals with exposed {0 0 1} facets

Yang Zheng[a], Kangle Lv[a,b,*], Zhouyou Wang[a], Kejian Deng[a,**], Mei Li[a]

[a] Key Laboratory of Catalysis and Materials Science of the State Ethnic Affairs Commission & Ministry of Education, South-Central University for Nationalities, Wuhan 430074, PR China

[b] State Key Laboratory of Advanced Technology for Materials Synthesis and Processing, Wuhan University of Technology, Wuhan 430070, PR China

ARTICLE INFO

Article history:
Received 30 September 2011
Received in revised form
30 December 2011
Accepted 9 January 2012
Available online 17 January 2012

Keywords:
Titania
Photocatalytic activity
{0 0 1} Facet
Surface fluorination

ABSTRACT

Anatase TiO_2 nanocrystals with tunable percentage of reactive {0 0 1} facets were rapidly synthesized by a microwave-assisted hydrothermal treatment of the mixed solution of tetrabutyl titanate (20 g), HF solution (3 ml) and additional water (0–21 g) at 200 °C for 30 min. The resulted sample is denoted as W*x*, where *x* represents the volumes of additional water. The photocatalysts were characterized by X-ray diffraction, transmission electron microscopy, nitrogen adsorption–desorption isotherms and X-ray photoelectron spectroscopy. The photocatalytic activity of the photocatalyst was evaluated by degradation of brilliant red X3B (X3B), an anionic dye, and by a photoluminescence technique using coumarin as a probe molecule. With increasing the amount of additional water from 0 to 21 ml, the shapes of TiO_2 nanocrystals evolve from nanosheets to truncated octahedral bipyramids, resulting in a steady decrease in the percentage of exposed {0 0 1} facets (from 71% to 23%). The photocatalytic activity of the resulted surface fluorinated TiO_2 nanocrystals increases first and then decrease with increase in the amount of water, and W3 sample with exposed 60% of {0 0 1} facets shows the highest photocatalytic activity. However, for the surface clean TiO_2 samples by washing with NaOH solution, W9 with 51% of {0 0 1} facets shows the highest photocatalytic activity. Our experimental results reflect that both crystal planes and surface chemistry play very important roles on the photocatalytic activity of anatase TiO_2 nanocrystals.

1. Introduction

Great efforts have been made to study semiconductor based photocatalysts due to their wide applications in environmental remediation and solar energy conversion [1–6]. Among which, TiO_2 photocatalysis has attracted increasing attention due to its biological and chemical inertness, strong photo oxidization power, cost effectiveness, and long-term stability against photo and chemical corrosion. However, the efficiency of TiO_2 photocatalysis still need to be further improved for practical application. Up to now, many methods, such as doping [7,8], noble metal deposition [9], surface modification [10–12], and semiconductor coupling [13,14], have been used to improve the efficiency. Many studies also showed that the morphology of TiO_2 play an important role on its efficiency [15,16].

The surface energies of its (0 0 1) and (1 0 1) facets have been calculated to be 0.90 and 0.44 J m^{-2}, respectively [17]. Therefore, anatase nanocrystals are usually observed in a truncated bipyramidal shape dominated by energetically stable (1 0 1) facets. By reversing the relative stability of {1 0 1} and {0 0 1} facets using HF as shape-direction reagent, Lu and co-workers reported the hydrothermal synthesis of high reactive anatase TiO_2 microcrystals with 47% {0 0 1} facets on the surface at 180 °C for 20 h [18]. Inspired by their outstanding work, many papers on the controllable synthesis of micro- or nanocrystalline TiO_2 with a large percentage of reactive facets, such as {0 0 1} [19–21], {0 1 0} [22], {1 0 0} [23] and {1 1 0} [24] have recently been published. Zhang et al. reported the synthesis of anatase TiO_2 microspheres with exposed mirror-like plane {0 0 1} facets by hydrothermal method using metal titanium foil as Ti source and HF solution at 180 °C for 3 h [25]. Dai et al. reported the synthesis of anatase TiO_2 nanocrystals with exposed {0 0 1} facets by hydrothermal treatment of electrospun nanofibers consisting of amorphous TiO_2 and poly(vinyl pyrrolidone) at 150 °C for 20 h [26]. Chen et al. demonstrated a facile approach for creating hierarchical spheres from large ultrathin anatase TiO_2 nanosheets with nearly 100% exposed (0 0 1) facets by hydrothermal reaction

* Corresponding author at: Key Laboratory of Catalysis and Materials Science of the State Ethnic Affairs Commission & Ministry of Education, South-Central University for Nationalities, Wuhan 430074, PR China. Tel.: +86 27 67843930; fax: +86 27 67842752.
** Corresponding author. Tel.: +86 27 67843930; fax: +86 27 67842752.
E-mail addresses: lvkangle@mail.scuec.edu.cn (K.L. Lv), Dengkj@scuec.edu.cn (K.J. Deng).

1381-1169/$ – see front matter © 2012 Elsevier B.V. All rights reserved.
doi:10.1016/j.molcata.2012.01.006

Table 1
Starting materials and the related physical properties of the photocatalysts.

Catalyst	Starting materials			Nitrogen adsorption–desorption characterization results			Relative crystallinity[a]	A/B	S_{001}%
	TBT (g)	HF (ml)	Water (ml)	S_{BET} (m^2/g)	PV (cm^3/g)	APS (nm)			
W0	20	3	0	82.7	0.11	5.5	1	–	71
W3	20	3	3	68.0	0.18	10.4	1.86	0.895	60
W9	20	3	9	72.8	0.14	7.9	1.75	0.857	51
W15	20	3	15	80.8	0.13	6.6	1.65	0.750	32
W21	20	3	21	95.3	0.11	4.7	0.75	0.667	23

[a] The relative crystallinity is evaluated via the relative intensity of anatase (1 0 1) plane diffraction peak using W0 sample as reference.

of the mixed solution of titanium(IV) isopropoxide and diethylenetriamine at 200 °C for 24 h [17]. Our group also reported the shape control and photocatalytic activity of high-energy anatase TiO_2 prepared by hydrothermal reaction of tetrabutyl titanate (TBT) and HF solution at 200 °C for 24 h, and it was found that the photocatalytic activity of high-energy anatase TiO_2 nanocrystals is positively related to the percentage of exposed {0 0 1} facets (6–96%) [19].

Photocatalytic reaction usually takes place on the surface of TiO_2. Therefore, the superficial inorganic species and organic adsorbates in TiO_2 play important role on the photocatalytic activity [27–29]. It was well documented that surface fluorination can enhance the photocatalytic activity of TiO_2 due to the formation of free hydroxyl radicals, which are more mobile than those generated on pure TiO_2 under UV irradiation (Eqs. (1) and (2)) [6,10,30,31]:

$$\equiv Ti{-}OH + h_{vb}{}^{+} \rightarrow \equiv Ti{-}OH^{\bullet +}(^{\bullet}OH_{ads}) \quad (1)$$

$$\equiv Ti{-}F + H_2O + h_{vb}{}^{+} \rightarrow \equiv Ti{-}F + {}^{\bullet}OH_{free} + H^{+} \quad (2)$$

The study of Han et al. found that the degradation efficiency of TiO_2 nanosheets after cleaning with alkaline solution was remarkably improved, because the adsorbed fluoride ions on the surface TiO_2 nanosheets can result in the hindrance adsorption of the dye [27]. However, our previous study showed that surface fluorination plays a positive role on the photocatalytic activity of the high-energy anatase TiO_2 nanocrystals with exposed {0 0 1} facets [19]. Hollow TiO_2 spheres (HTS) with exposed 20% {0 0 1} facets were synthesized by Liu et al. by a fluoride mediated self-transformation method [32]. They found that surface chemistry and the surface structure at the atomic level are key factors in tuning the adsorption selectivity and, consequently, photocatalytic selectivity of HTS toward azo dyes. The fluorinated HTS show preferential decomposition of methyl orange (MO) in comparison to methylene blue (MB). However, the surface-modified HTS by NaOH washing favor decomposition of MB over MO. Therefore, the reasons for the different effect of surface fluorination on the photocatalytic activity of high-energy TiO_2 nanosheets needs to be further studied.

Microwave-assisted fabrication of TiO_2 can reduce the time required for the synthesis and increase the crystallinity of the product [33–35]. Solvents which are polar in nature have a good potential to adsorb microwaves and convert them to thermal energy, thus accelerating the reactions as compared to results obtained using conventional heating. Visible-light-driven plasmonic photocatalyst Ag–TiO_2 nanocomposite hollow spheres have been prepared under microwave-hydrothermal conditions at 180 °C for 1 h [34]. Although the hydrothermal/solvothermal approaches have shown their advantages in the fabrication of TiO_2 with reactive facets, they are not an energy-efficient process due to the long reaction time involved. Recently, Zhang et al. reported the synthesis of micrometer-size anatase TiO_2 single-crystals with chemically reactive {0 0 1} facets at 210 °C for only 90 min by using a microwave-assisted method [33,35]. However, to the best of knowledge, microwave-assisted synthesis of anatase TiO_2 nanocrystals with exposed reactive {0 0 1} facets has not been reported yet.

Herein we report on the rapid synthesis of anatase TiO_2 nanocrystals with a continuously tunable percentage of reactive {0 0 1} facets via a microwave enhanced thermal approach at 200 °C for 30 min using TBT and HF solution as starting materials. The relationship between the physicochemical properties and the photocatalytic performance of the samples is discussed.

2. Experimental

2.1. Sample preparation

3.0 ml HF solution (40 wt.%) was diluted with certain amount of water, followed by dropwise added into 20 g of TBT under magnetic stirring. The mixture was sealed in a Teflon-lined double-walled digestion vessel. After treatment at 200 °C for 30 min using a microwave digestion system (MDS-6, Sineo, Shanghai, China), the vessel was then cooled down to room temperature. The products were washed with ethanol for 2 times to remove organic impurities, then filtrated through a membrane filter (pore size, 0.45 μm), and thoroughly rinsed with distilled water until the pH value of the filtrate is about 7. Then the precipitates were dried in a vacuum oven at 80 °C for 6 h. The resulted sample is denoted as W*x*, where *x* represents the volumes of additional water added to HF solution (Table 1).

2.2. Characterization

The X-ray diffraction (XRD) patterns obtained on a D8-advance X-ray diffractometer (German Bruker). The accelerated voltage and applied current were 15 kV and 20 mA, respectively. The average crystalline size of the catalyst was determined according to the Scherrer equation using full width at half maximum data after correcting for the instrumental broadening. Transmission electron microscopy (TEM) observations were carried out on a Tecnai G20 microscope using an acceleration voltage of 200 kV. The BET surface area (S_{BET}), pore volume (PV) and average pore size (APS) of the powders were analyzed by using nitrogen adsorption in a nitrogen-adsorption apparatus (Micromeritics ASAP 2020, USA). All the samples were degassed at 150 °C prior to the nitrogen-adsorption measurements. X-ray photoelectron spectroscopy (XPS) measurements were done with a Kratos XSAM800 XPS system with Mg Kα source and a charge neutralizer, all the binding energies were referenced to the C 1s peak at 284.8 eV of the surface adventitious carbon.

2.3. Photocatalytic degradation

The light source (375 W, Shanghai Yamin) emitted mainly at 365 nm, and placed outside a Pyrex-glass reactor at a fixed distance (ca. 10 cm) [12]. During the photocatalytic reaction, the reactor was maintained at room temperature through a water recycle system, and was mechanically stirred at a constant rate. The concentration of TiO_2 was 1.0 g/L, and the initial concentration of X3B (Fig. 1)

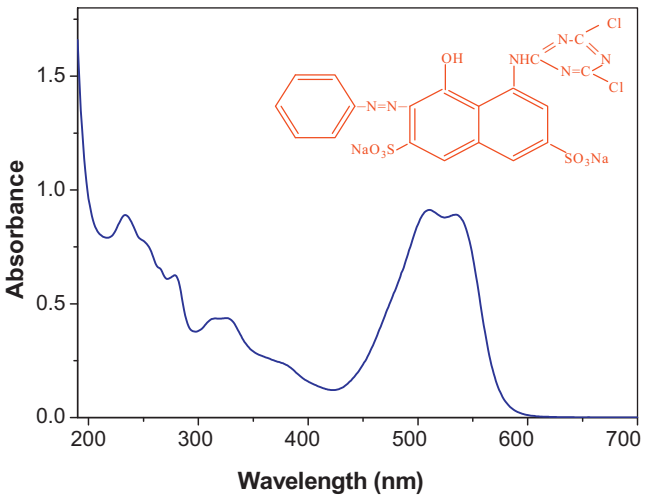

Fig. 1. Structure and electronic absorption spectrum of X3B in water.

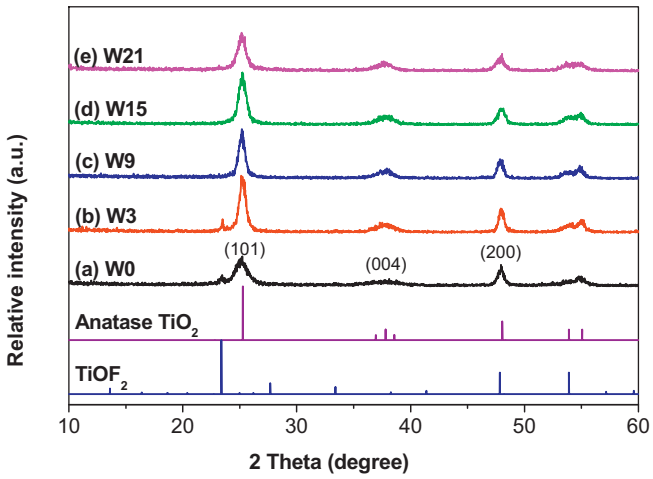

Fig. 2. XRD patterns of the photocatalysts, together with the expected diffraction peaks for anatase TiO_2 and $TiOF_2$.

was 1.0×10^{-4} mol/L. Before irradiation, the suspensions were sonicated first for 5 min, and then were shaken overnight in the dark. At given intervals of irradiation, small aliquots were withdrawn by a syringe, and filtered through a membrane (pore size 0.45 μm). The concentration of X3B remaining in the filtrate was then analyzed by an Agilent 8451 spectrometer at 510 nm.

2.4. Determination of free •OH radicals

The analysis of the formation of free •OH radicals, produced in suspensions high-energy anatase TiO_2 nanocrystals under UV irradiation, was performed by photoluminescence (PL) technique using coumarin as a probe molecule, which readily reacted with •OH radicals to produce highly fluorescent product, 7-hydroxycoumarin [36,37]. Sampling was performed in every 2 min. Solution after filtration through 0.45 μm membrane filter was analyzed on a Hitachi F-7000 fluorescence spectrophotometer by the excitation with the wavelength of 332 nm [19].

3. Results and discussion

3.1. Phase structure and morphology

Fig. 2 shows the XRD patterns of the photocatalysts. A broad peak at $2\theta = 25.3^\circ$ corresponding to the (1 0 1) plane diffraction of anatase TiO_2 (JCPDS No. 21-1272) was observed for all the

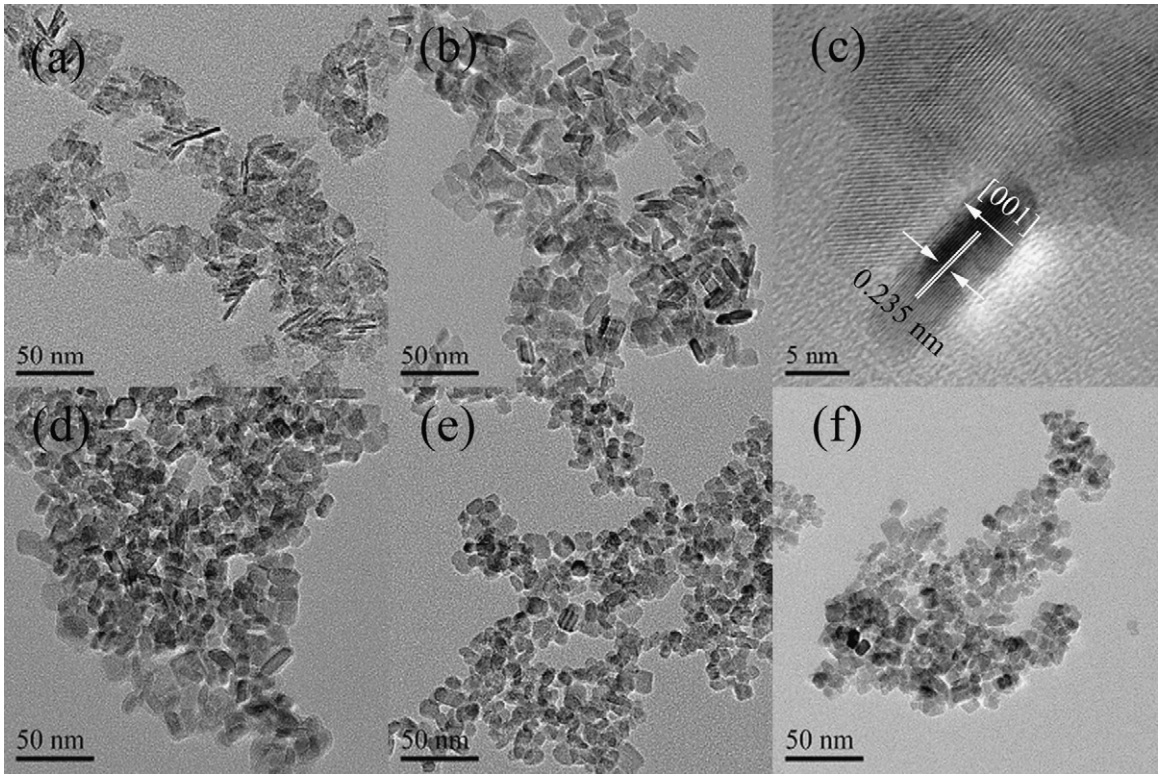

Fig. 3. TEM images of W0 (a), W3 (b and c), W9 (d), W15 (e) and W21 (d) samples, respectively. The high-resolution TEM image of W3 (c) directly showed that the lattice spacing parallel to the top and bottom facets was 0.235 nm, corresponding to the (0 0 1) planes of anatase TiO_2.

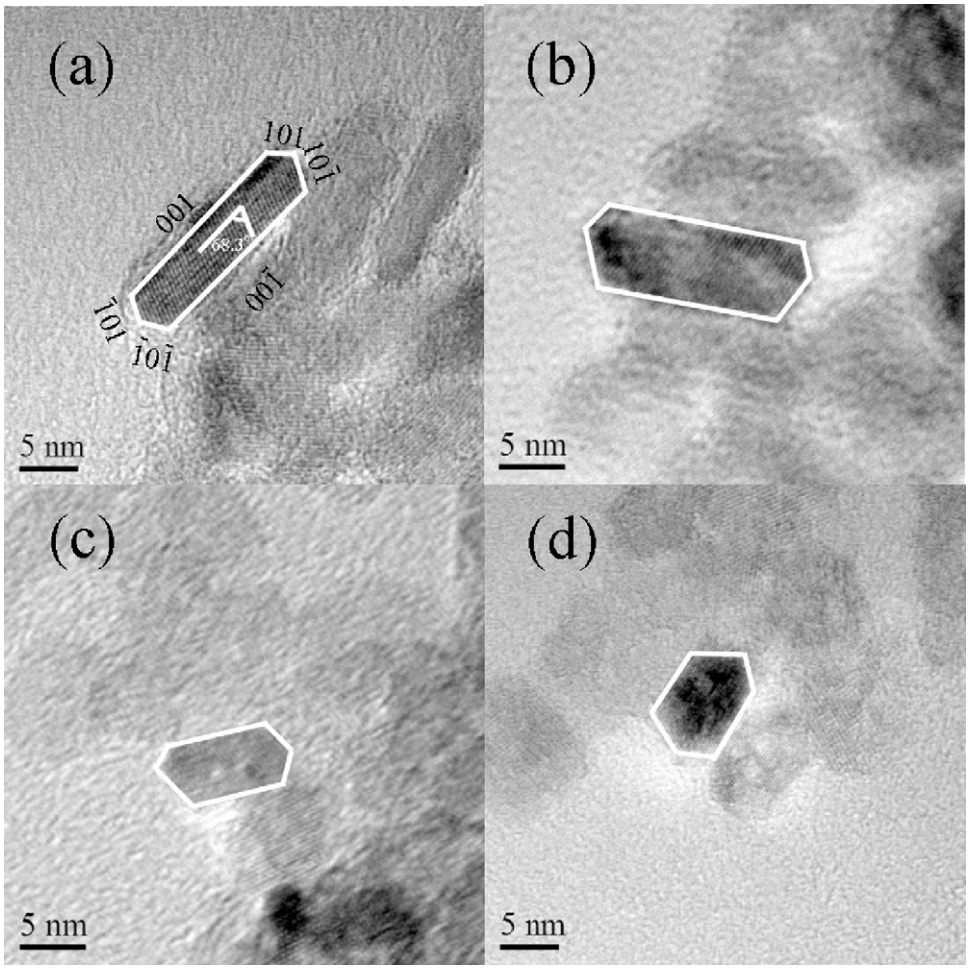

Fig. 4. High-resolution TEM images of W3 (a), W9 (b), W15 (c) and W21 (d) samples, respectively.

photocatalysts [38]. The broadening of the diffraction peak is caused by weak crystallization of W0 sample. Interestingly, a small peak at $2\theta = 23.5^\circ$, corresponding to the (1 0 0) peak of $TiOF_2$ (JCPDS No. 01-0490), was also detected for W0 photocatalyst. It has been reported that $TiOF_2$ can be formed in high concentrated HF solution [19,39]. According to our experimental results, $TiOF_2$ shows very poor photocatalytic activity [19]. When additional 3 ml of water was added, the peak intensity of anatase (1 0 1) increases, indicating an enhancement of crystallization of W3 sample (Fig. 1b). This is ascribed to the extensive hydrolysis of TBT in water. However, further increase in the amount of water, the intensity of the peak begins to decline due to the low concentration of TBT in solution. The relative crystallinity of anatase TiO_2 sample firstly increases and then decreases with increasing the amount of additional water, and W3 sample shows the best crystallinity among all the photocatalysts (Table 1).

TEM images of the as-prepared samples are shown in Fig. 3. From Fig. 3a, it can be seen that rectangular sheet-like anatase TiO_2 nanocrystals, with a width of about 15 nm and a thickness of 3 nm, were obtained in high concentrated HF solution (W0). The morphology of W0 is similar to the TiO_2 nanosheets with exposed high-energy {0 0 1} facets prepared by ordinary hydrothermal reaction [19,27]. When additional 3 ml of water was added (W3 sample), the width of the obtained nanosheets increases to about 18 nm and the thickness increases to 4.5 nm (Fig. 3b). The high-resolution TEM image of W3 directly showed that the lattice spacing parallel to the top and bottom facets was about 0.235 nm, corresponding to the (0 0 1) planes of anatase TiO_2 (Fig. 3c). With further increase in the amount of water, the thickness of the sample slowly increases and the width steadily decreases (Fig. 3d–f).

Fig. 4a shows a high-resolution TEM image of W3 sample. An angle of ca. 68.3° between two lattice directions, consistent with the interfacial angle between (0 0 1) and (1 0 1), is also observed on the hexagonal-shaped particle of W3, suggesting that the particle exhibits flat surfaces of {0 0 1} and {1 0 1}. Therefore, W3 is characterized by a truncated octahedronal bipyramid which is enclosed by eight equivalent {1 0 1} facets and two equivalent {0 0 1} facets (Fig. 4a). The morphology of anatase TiO_2 single-crystals can be defined in terms of two independent length parameters. The side of the bipyramidal is denoted A, and the side of the "truncation" facets is denoted B (inset of Fig. 5). The degree of truncation may therefore be described by the size of B with respect to A (where $B \leq A$) [18]. The ratio of reactive {0 0 1} facets to the total surface area therefore can be described by S_{001}/S_{total} (S_{001}%) or the value of B/A. With increase in the amount of additional water, the width of the samples decrease while the thickness increases (Fig. 4), resulting in a decrease in the value of B/A (or S_{001}%) (Table 1). The calculation method on the percentage of exposed {0 0 1} facets can be found in literatures [21,33,40].

Fig. 5 shows the relationship between average crystalline sizes of the photocatalysts (along [1 0 0] and [0 0 1] directions) and the amount of additional water used. It can be seen that the crystalline sizes along [0 0 1] direction slightly increase with increasing the amount of water, but the crystalline sizes along {1 0 0] direction increase first and then decrease, which confirms the preferential growth of TiO_2 nanocrystals along c-axis on the expense of growth

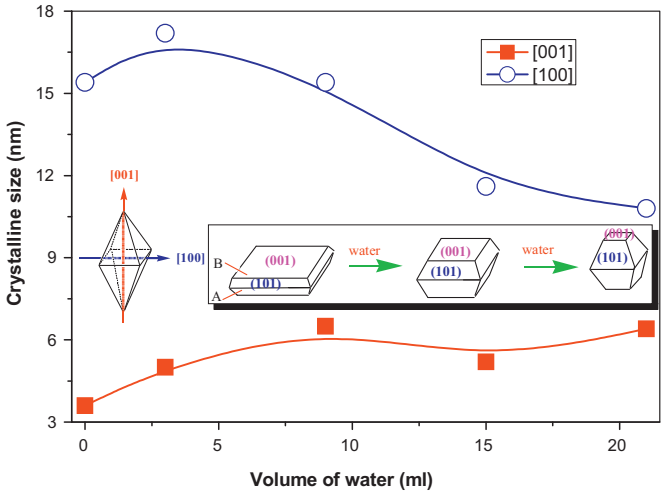

Fig. 5. Dependence of average crystalline sizes of the photocatalysts along [0 0 1] and [1 0 0] direction on the amount of water, indicating that the photocatalyst slightly increases along *c*-axis ([0 0 1] direction), while the growth along *a*-axis ([1 0 0] direction) is restrained (inset is the corresponding shape simulation).

along *a*-axis (inset of Fig. 5). These results are consistent with TEM images shown in Figs. 3 and 4.

3.2. BET surface areas and pore distributions

Fig. 6 shows nitrogen adsorption–desorption isotherms and the corresponding pore size distribution curves (inset) of W0, W3 and W15 of TiO_2 samples, respectively. It can be seen that these powders have isotherms of type IV with type H2 hysteresis loops, which can be observed in the ink-bottle-like pores with narrow necks and wider bodies [41]. The pore size distribution calculated from the desorption branch of the nitrogen isotherm by the BJH (Barrett–Joyner–Halenda) method shows narrow range for all the samples. The maximum pore diameter of the photocatalyst increase first and then decreases, and W3 shows the largest APS of 10.4 nm (inset of Fig. 6) due to it well crystallization (Fig. 1b). These mesopores are from the aggregation of primary particles. The narrow pore distributions also imply that the prepared TiO_2 particles have a relatively uniform particle size distribution (Fig. 3) [18], indicating that microwaves can provide rapid and uniform heating of reagent and solvents. The homogeneous microwave heating therefore provides uniform nucleation and growth conditions,

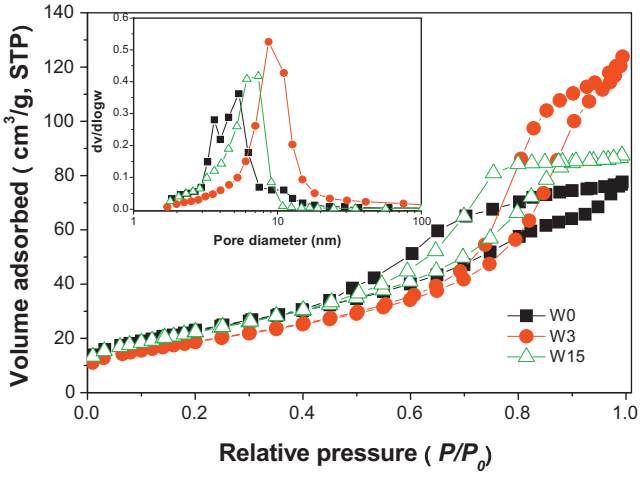

Fig. 6. Nitrogen adsorption–desorption isotherms and the corresponding pore size distributions (inset) of W0, W3 and W15 photocatalysts, respectively.

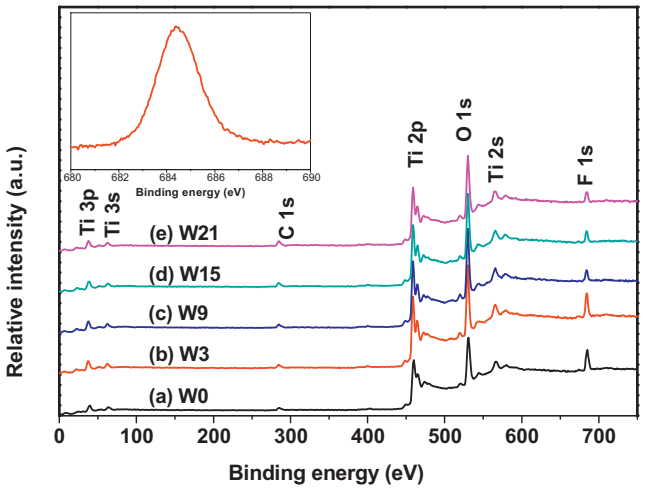

Fig. 7. XPS survey spectra of the photocatalysts. Inset is the corresponding high-resolution F1s XPS spectrum of W3 sample.

which results in the formation of anatase TiO_2 nanocrystals with a narrow size distribution [33].

3.3. XPS analysis

Fig. 7 shows XPS survey spectra of the TiO_2 samples. All the sample contains not only Ti, O and C, but also F elements, with sharp photoelectron peaks appearing at binding energies of 684 (F1s), 458 (Ti2p), 531 (O1s), and 285 eV (C1s). The carbon peak is attributed to the residual carbon from the sample and adventitious hydrocarbon from the XPS instrument itself, and F element come from HF solution.

Inset of Fig. 7 shows a typical high-resolution XPS spectrum of the F 1s region, taken on the surface of W3 powders. According to our previous results as well as literatures [19,30,42], the F1s peak at 684 eV is due to the surface fluoride (≡Ti—F) or $TiOF_2$ phase, consistent with the XRD results (Fig. 2). No signal of F^- ions in the lattice (binding energy of 688.5 eV) was found. The molar ratios of F to Ti decreases from 69.5% (W0) to 27.6% (W21) with increase in the amount of additional water.

Surface fluorination can affect the photocatalytic activity of high-energy TiO_2 nanocrystals [27,43], which will be shown below.

3.4. Photocatalytic activity

It was reported that anatase TiO_2 nanocrystals with exposed reactive {0 0 1} facets showed high photocatalytic activity [32,44–46]. Here X3B was used as the target organic pollutant to test the photocatalytic activity of the reactive anatase TiO_2 samples. Fig. 8A shows the degradation profiles of X3B in suspensions of different photocatalyst under other identical situations. It can be seen that X3B is a very stable organic chemical, which shows little degradation under mercury light ($\lambda \geq 320$ nm) in the absence of the photocatalyst [47]. However, in the presence of the photocatalyst, X3B shows obvious degradation. The kinetic data for the degradation of X3B can be well fitted by the apparent first-order rate equation, and the comparison of the rate constants can be seen in Fig. 8B. It can be seen that the photocatalytic activity of TiO_2 nanocrystals increases first and then decreases with increase in the amount of water, and W3 shows the highest photocatalytic activity (0.021 min^{-1}), reflecting the synergistic effect between {0 0 1} and other facets on the photocatalytic activity of high-energy anatase TiO_2.

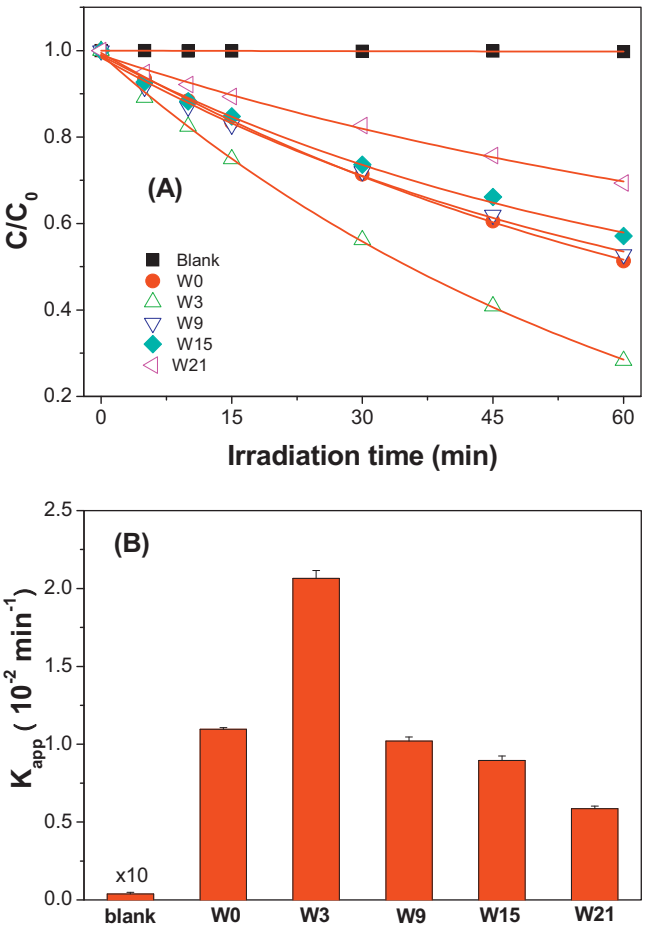

Fig. 8. Degradation time profiles of X3B in different photocatalysts (A) and the corresponding rate constants (B).

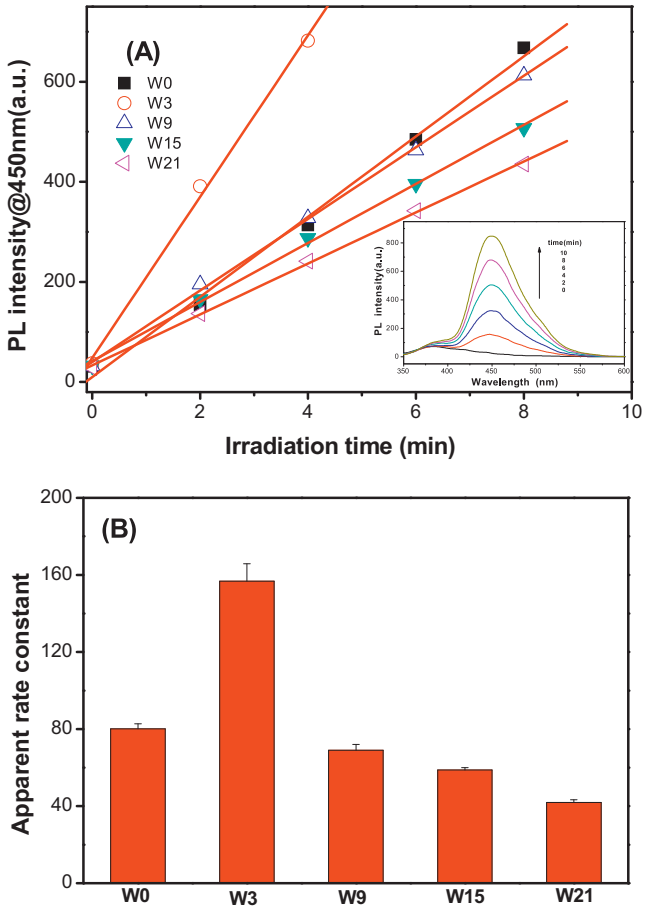

Fig. 9. Time dependence of the induced photoluminescence intensity @ 450 nm of the photocatalysts (A) and the related rate constants (B). Inset of (A) is the photoluminescence spectral changes observed during illumination of W0 TiO_2 suspensions.

Considering that the dye can be degraded through photosensitization pathway, the formation of photo-induced •OH radicals, one of the most important reactive oxygen species, in TiO_2 suspensions were also measured using a PL technical. Here coumarin is selected as a probe molecule, which readily reacted with •OH radicals to produce highly fluorescent product, 7-hydroxycoumarin [36,48]. Inset of Fig. 9A shows the typical PL spectral changes observed during illumination of the suspensions of W0. The PL intensity of photo-generated 7-hydroxycoumarin at 450 nm (excited at 332 nm) increases with irradiation time, obeying a pseudo-zero-order reaction rate equation in kinetics (Fig. 9A), and the corresponding PL formation rate constants are shown in Fig. 9B. It can be seen that W3 also shows the highest photocatalytic activity on the formation of •OH radicals with a rate constant of 156.8, which is much more active than TiO_2 nanosheets with exposed similar percentage of {0 0 1} factes synthesized by traditional hydrothermal reaction (the rate constant for HF4 sample with exposed 63% {0 0 1} facets is 48.4) [19].

To study the effect of surface fluoride ions on the photoactivity of TiO_2 nanosheets with exposed {0 0 1} facets, the fluorinated surface of TiO_2 nanosheets was cleaned by washing with NaOH diluted solution. It has been reported that the adsorbed fluoride ions on the surface of TiO_2 can be easily removed by alkaline washing in a NaOH solution without altering the crystal structure and morphology [42]. This is due to the fact that F^- on the surface of TiO_2 nanosheets is removed by a simple ligand exchange reaction between OH^- in the NaOH solution and F^- on TiO_2 (Eq. (3)).

$$\equiv Ti{-}F + OH^- \leftrightarrow \equiv Ti{-}OH + F^- \quad (3)$$

In this study, the fluorinated TiO_2 nanocrystals were first washed by 0.1 mol/L diluted NaOH solution one time, then washed by distilled water three times. Fig. 10 shows the comparison of the photocatalytic activity of high-energy TiO_2 nanocrystals before and after washed by NaOH. It can be seen that, different from surface fluorinated TiO_2 nanocrystals, W9 with exposed 51% {0 0 1} facets shows the highest photocatalytic activity (0.028 min^{-1}) among all the surface clean TiO_2 nanocrystals. Surface fluorination plays a positive role for W0 and W3 samples. However, negative effect of

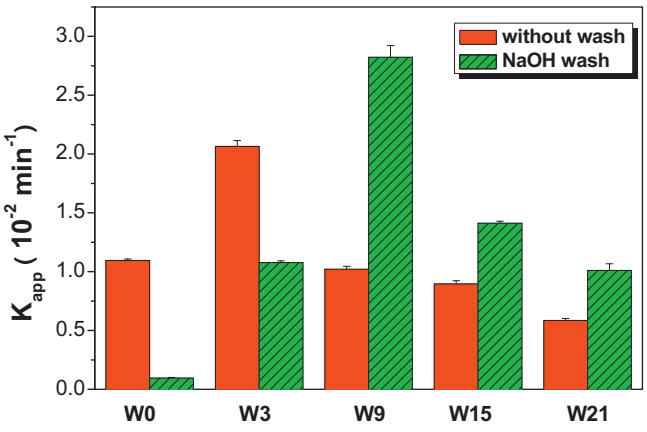

Fig. 10. Comparison of the degradation rate constants of X3B in the presence of different photocatalysts before and after washed by 0.1 mol/L NaOH solution.

surface fluorination was observed for W9, W15 and W21 samples. After washed by NaOH, the photocatalytic activity of W3 and W9 decreased 47.6% and increased 180%, respectively (Fig. 10). With increase in the percentage of exposed {0 0 1} facets, the positive effect of fluoride ions on the photocatalytic activity of high-energy TiO_2 nanocrystals becomes more obvious. The positive effect of fluoride effection was attributed to the formation of free hydroxyl radicals (Eq. (2)) [19,42], while the negative effect of fluoride effection was ascribed to the hindrance adsorption of the dye due to the competitive adsorption between dye and fluoride ions. We have studied the effect of phase structure of TiO_2 on fluoride effection [31]. The relationship between exposed high-energy facets and fluoride effection needs to be further studied.

4. Conclusions

Anatase TiO_2 nanocrystals with tunable percentage of reactive {0 0 1} facets were rapidly synthesized via a microwave-assisted process using TBT as titanium source and HF as shape-direction reagent. Both the exposed facets and surface chemistry play important roles on the photocatalytic activity of anatase TiO_2 nanocrystals. This study may provide new insight into design and preparation of advanced photocatalytic materials.

Acknowledgements

This work was supported by the National Natural Science Foundation of China (20977114 & 20977115), Natural Science Foundation of Hubei Province (2010CDA068 & 2011CDA107) and China Postdoctoral Science Foundation (201003500).

References

[1] A. Fujishima, K. Honda, Nature 238 (1972) 37–38.
[2] X.B. Chen, S.S. Mao, Chem. Rev. 107 (2007) 2891–2959.
[3] J. Wang, D.N. Tafen, J.P. Lewis, Z. Hong, A. Manivannan, M.J. Zhi, M. Li, N.Q. Wu, J. Am. Chem. Soc. 131 (2009) 12290–12297.
[4] J.H. Pan, X.W. Zhang, A.J. Du, D.D. Sun, J.O. Leckie, J. Am. Chem. Soc. 130 (2008) 11256–11257.
[5] K.L. Lv, J.G. Yu, J.J. Fan, M. Jaroniec, CrystEngComm 14 (2011) 7044–7048.
[6] X.J. Xue, Q. Sun, Y. Wang, K.L. Lv, Y.M. Xu, Acta Chim. Sin. 68 (2010) 471–475.
[7] F. Asahi, T. Morikawa, T. Ohwaki, K. Aoki, Y. Taga, Science 293 (2001) 269–271.
[8] S.U.M. Khan, M. Al-Shahry, W.B. Ingler Jr., Science 297 (2002) 2243–2245.
[9] B. Sun, A.V. Vorontsov, P.G. Smirniotis, Langmuir 19 (2003) 3151–3156.
[10] C. Minero, G. Mariella, V. Maurino, E. Pelizzetti, Langmuir 16 (2000) 2632–2641.
[11] C.C. Chen, P.X. Lei, H.W. Ji, W.H. Ma, J.C. Zhao, H. Hidaka, N. Serpone, Environ. Sci. Technol. 38 (2004) 329–337.
[12] K.L. Lv, Y.M. Xu, J. Phys. Chem. B 110 (2006) 6204–6212.
[13] K. Vinodgopal, P.V. Kamat, Environ. Sci. Technol. 29 (1995) 841–845.
[14] L.X. Yang, S.L. Luo, Y. Li, Y. Xiao, Q. Kang, Q.Y. Cai, Environ. Sci. Technol. 44 (2010) 7641–7646.
[15] J.G. Yu, S.W. Liu, H.G. Yu, J. Catal. 249 (2007) 59–66.
[16] K.L. Lv, Q.J. Xiang, J.G. Yu, Appl. Catal. B 104 (2011) 275–281.
[17] J.S. Chen, Y.L. Tan, C.M. Li, Y.L. Cheah, D. Luan, S. Madhavi, F. Boey, L.A. Archer, X.W. Lou, J. Am. Chem. Soc. 132 (2010) 6124–6130.
[18] H.G. Yang, C.H. Sun, S.Z. Qiao, J. Zou, G. Liu, S.C. Smith, H.M. Cheng, G.Q. Lu, Nature 453 (2008) 638–641.
[19] Z.Y. Wang, K.L. Lv, G.H. Wang, K.J. Deng, D.G. Tang, Appl. Catal. B 100 (2010) 378–385.
[20] G. Liu, H.G. Yang, X.W. Wang, L. Cheng, J. Pan, G.Q. Lu, H.M. Cheng, J. Am. Chem. Soc. 131 (2009) 12868–12869.
[21] J. Zhu, S.H. Wang, Z.F. Bian, S.H. Xie, C.L. Cai, J.G. Wang, H.G. Yang, H.X. Li, CrystEngComm 12 (2010) 2219–2224.
[22] B.H. Wu, C.Y. Guo, N.F. Zheng, Z.X. Xie, G.D. Stucky, J. Am. Chem. Soc. 130 (2008) 17563–17567.
[23] J.M. Li, D.S. Xu, Chem. Commun. 46 (2010) 2301–2303.
[24] M. Liu, L.Y. Piao, L. Zhao, S. Ju, Z.J. Yan, T. He, C.L. Zhou, W.J. Wang, Chem. Commun. (2010) 1664–1666.
[25] J.G. Yu, J.J. Fan, K.L. Lv, Nanoscale 2 (2010) 2144–2149.
[26] Y.Q. Dai, C.M. Cobley, J. Zeng, Y.M. Sun, Y.N. Xia, Nano Lett. 9 (2009) 2455–2459.
[27] X.G. Han, Q. Kuang, M.S. Jin, Z.X. Xie, L.S. Zheng, J. Am. Chem. Soc. 131 (2009) 3152–3153.
[28] Y.M. Xu, K.L. Lv, Z.G. Xiong, W.H. Leng, W.P. Du, D. Liu, X.J. Xue, J. Phys. Chem. C 111 (2007) 19024–19032.
[29] M. Liu, K.L. Lv, G.H. Wang, Z.Y. Wang, Y.X. Zhao, Y.R. Deng, Chem. Eng. Technol. 33 (2010) 1531–1536.
[30] H. Park, W. Choi, J. Phys. Chem. B 108 (2004) 4086–4093.
[31] K.L. Lv, X.F. Li, K.J. Deng, J. Sun, X.H. Li, M. Li, Appl. Catal. B 95 (2010) 383–392.
[32] S.W. Liu, J.G. Yu, M.T. Jaroniec, J. Am. Chem. Soc. 132 (2010) 11914–11916.
[33] D.Q. Zhang, G.S. Li, H.B. Wang, K.M. Chan, J.C. Yu, Cryst. Growth Des. 10 (2010) 1130–1137.
[34] Q.J. Xiang, J.G. Yu, B. Cheng, H.C. Ong, Chem. Asian J. 5 (2010) 1466–1474.
[35] D.Q. Zhang, G.S. Li, X.F. Yang, J.C. Yu, Chem. Commun. (2009) 4381–4383.
[36] K. Ishibashi, A. Fujishima, T. Watanabe, K. Hashimoto, Electrochem. Commun. 2 (2000) 207–210.
[37] H.M. Guan, L.H. Zhu, H.H. Zhou, H.Q. Tang, Anal. Chim. Acta 608 (2008) 73–78.
[38] K.L. Lv, J.G. Yu, K.J. Deng, J. Sun, Y.X. Zhao, D.Y. Du, M. Li, J. Hazard. Mater. 173 (2010) 539–543.
[39] J. Zhu, D.Q. Zhang, Z.F. Bian, G.S. Li, Y.N. Huo, Y.F. Lu, H.X. Li, Chem. Commun. (2009) 5394–5396.
[40] J.G. Yu, G.P. Dai, Q.J. Xiang, M. Jaroniec, J. Mater. Chem. 21 (2011) 1049–1057.
[41] J.G. Yu, W.G. Wang, B. Cheng, B.L. Su, J. Phys. Chem. C 113 (2009) 6743–6750.
[42] Q.J. Xiang, K.L. Lv, J.G. Yu, Appl. Catal. B 96 (2010) 557–564.
[43] G. Liu, J.C. Yu, G.Q. Lu, H.M. Cheng, Chem. Commun. 47 (2011) 6763–6783.
[44] H.G. Yang, G. Liu, S.Z. Qiao, C.H. Sun, Y.G. Jin, S.C. Smith, J. Zou, H.M. Cheng, G.Q. Lu, J. Am. Chem. Soc. 131 (2009) 4078–4083.
[45] S.W. Liu, J.G. Yu, M. Jaroniec, Chem. Mater. (2011) 4085–4093.
[46] J.G. Yu, L.F. Qi, M. Jaroniec, J. Phys. Chem. C 114 (2010) 13118–13125.
[47] Y. Zheng, K.L. Lv, X.F. Li, K.J. Deng, J. Sun, L.Q. Chen, L.Z. Cui, D.Y. Du, Chem. Eng. Technol. 34 (2011) 1630–1634.
[48] K.L. Lv, J.G. Yu, K.J. Deng, X.H. Li, M. Li, J. Phys. Chem. Solid 71 (2010) 519–522.